Solar hydrogen generation from ambient humidity using functionalized porous photoanodes

Georgios Zafeiropoulos[1], Hannah Johnson[2], Sachin Kinge[2], Mauritius C.M. van de Sanden[1,3],

Mihalis N. Tsampas[1,*]

[1]*Dutch Institute For Fundamental Energy Research - DIFFER, Eindhoven, 5612AJ, the Netherlands*

[2]*TOYOTA MOTOR EUROPE NV/SA, Hoge Wei 33, 1930 Zaventem, Belgium*

[3]*Department of Applied Physics, Eindhoven University of Technology, 5600 MB, Eindhoven, The Netherlands*

*m.tsampas@differ.nl

ABSTRACT

Solar hydrogen is a promising sustainable energy vector and steady progress has been made in the development of photoelectrochemical cells. Most research in this field has focused on using acidic or alkaline liquid electrolytes for ionic transfer. However, the performance is limited by (i) scattering of light and blocking of catalytic sites by gas bubbles and (ii) mass transport limitations. An attractive alternative to a liquid water feedstock is to use the water vapor present as humidity in ambient air, which has been demonstrated to mitigate the above problems and can expand the geographical range where these devices can be utilized.

We show here how the functionalization of porous TiO_2 and WO_3 photoanodes with solid electrolytes - proton conducting Aquivion® and Nafion® ionomers, enables the capture of water from ambient air and allows subsequent photoelectrochemical hydrogen production. The optimization strategy of the photoanode functionalization was examined through testing the effect of ionomer loading and the ionomer composition. Optimized functionalized photoanodes operating at 60% relative humidity (RH) and T_{cell}=30-70°C were able to recover up 90% of the performance obtained at 1.23 V vs RHE when water is introduced in liquid phase (i.e. conventional PEC operation). Full performance recovery is achieved at higher applied potential. In addition, long term experiments have shown remarkable stability at 60% RH for 64 h of cycling (8 h continuous illumination – 8 h dark) demonstrating that the concept can be applicable outdoors.

KEYWORDS: Photoelectrochemical water splitting, vapor phase operation, porous photoanodes, water capturing, Aquivion®, Nafion®

INTRODUCTION

One of the main challenges facing mankind in the twenty-first century is to supply the world's population with sufficient energy to meet the desired living standards[1]. To date, more than 85% of our energy needs are met by the combustion of fossil fuels, which can relatively easily be harvested from stocks of concentrated natural photosynthetic products: coal, oil, and natural gas[2]. However, the use of fossil fuels is accompanied by the emission of greenhouse gases, particularly carbon dioxide, which is the main cause of climate change[3]. To reduce our dependence on fossil fuels, we need to make a large-scale transition towards new, sustainable sources of energy[4].

To achieve a sustainable society, we need an energy mix primarily based on renewables, such as solar energy. Since sunlight is intermittent and seasonal, we need long-term methods for storing this energy, for example as chemical fuels[1,5]. The concept of photoelectrochemical (PEC) water splitting for hydrogen production combines the harvesting of solar energy and the electrolysis of water into a single device[6]. PEC devices use semiconductors to absorb sunlight, which generates electron–hole pairs. These electron-hole pairs separate and transport the charge carriers to the semiconductor/electrolyte interface for water splitting to hydrogen and oxygen[7]. In this way, intermittent solar energy is converted into an inherently more storable form of energy -that of chemical bonds[8].

State-of-the-art photoelectrochemical devices have achieved efficiencies of up to 19% but are largely based on III-V semiconductors photoelectrodes[1,9-11] which are expensive and based on scarce materials. On the other hand, oxide-based photoelectrodes[12-17] are attractive because of their inexpensive processing costs and better stability in aqueous media, but show a lower demonstrated performance. The commercial viability of a water splitting PEC will be ultimately determined by the cost of hydrogen produced which is typically considered to be a compromise between the material cost and STH efficiency. However, engineering efforts to optimize the design by limiting mass transport will also play a crucial part in realizing close to theoretical efficiencies in and reducing the cost of the future PEC installations.

Laboratory-scale PEC studies are usually performed in aqueous electrolyte solutions using purified water and simulated light illumination[1,8]. However, an attractive, alternative feedstock to liquid water is the water vapor present as humidity in the ambient air[18-22]. Capturing water from the air implies no liquid water is needed for operation, making it a "water neutral" process. This, potentially enables the construction of free-standing devices, in areas which don't usually have a nearby water supply i.e. near to roads or remote areas. In the oceans, where the water and sunlight resources are abundant, desalination and purification processes are crucial for liquid seawater splitting in order to avoid catalyst corrosion,

poisoning and fouling and by-product formation[20,21]. In comparison, water vapor splitting can be in-situ realized without any prior water treatment by placing the device above the water surface. In addition, gas phase water splitting minimizes the possibility of blocking catalytic sites or scattering light through bubble formation, and decreases the maintenance costs significantly because natural convection of air can be used to feed the water vapor. Therefore, systems to pump liquid water are not required[18-22]. Additionally this approach expands the range of geographical locations where these technologies can be applicable. For example: in low-cost land and abundant solar radiation areas, where stable supply of water might be problematic owing to limited rainfall[20,21].

Inspired by the polymeric electrolyte membrane (PEM) electrolysers, a few research groups[23-31] have attempted to separate the two electrochemical half-reactions with an ionically conductive polymeric membrane to accommodate water vapor-based operation. In the PEM-PEC design from our group, the two electrochemical half-reactions are separated by the solid electrolyte, sandwiched between porous substrates to facilitate the reactant/product transfer through the electrode towards the electrolyte[22,32]. In this design the hydrogen generation and water dissociation are taking place in different chambers meeting the operational requirements (i.e. one compartment exposed to ambient air). In our previous work[22-24], we have developed and implemented a unique PEM-PEC cell, which apart from the anodic and the cathodic chambers, is equipped with a reference electrode compartment. This allows reliable PEM-PEC photoelectrode characterization and benchmarking of the water vapor operation with the liquid operation (in conventional PEC cells). However, in our previous studies the photoelectrodes were evaluated at relative humidity (RH) higher than 100%, which implies that water condensation was taking place during water vapor operation[22-24].

Herein, we address the challenge of functionalizing porous photoanodes towards water vapor operation at RH from 0 to 100%. Stable, metal oxide photoanodes with reproducible performance were produced by a simple fabrication method (i.e. oxygen annealing of Ti or W porous substrates). Water vapor capturing was achieved impregnation of commercial perfluorosulfonic (PFSA) acid ionomers Nafion® (DuPont) or Aquivion® (Solvay) in our porous photoanodes. A systematic investigation on the effect of ionomer composition and loading was carried out to enable optimization of the functionalized photoanodes.

Although, the concept of gas phase operation of PEM-PEC cells has been already validated in literature[18-20,28], but no protocols yet exist for benchmarking the efficiency of PEM-PEC devices operating under (low RH) humidified air. We report a protocol for evaluating activity and stability, which can be applied to different photoanodes, both functionalized and bare, in PEM-PEC operation at various RH levels (0 –

100%) and temperatures (30 – 70 °C). In our unique set-up, it was also possible to compare the performance with conventional PEC designs where the photoanode is immersed in liquid water. To address durability issues, our protocol also involves evaluation of the stability under conditions relevant to outdoor application (at 60% RH for 64 h, cycling between 8 h continuous illumination- 8 h dark).

Overall, our results show that photoelectrochemical water splitting can be sustained by the humidity of ambient air, under various temperature and relative humidity combinations, when functionalized photoanodes are used. For example, by properly tuning the functionalization parameters and the photoanode microstructure, we managed, at 30 °C, 60% RH under 1.23 V, to recover up to 90% of the performance obtained when water is introduced in liquid phase. Isotopic labelling studies were performed to exclude that other parasitic side-reactions are taking place. Electrochemical impedance spectroscopy measurements confirmed that the proposed functionalization improves the water absorption and charge transfer during gas phase operation.Finally, in view of practical applications, we investigated the effect of prolonged UV and Vis illumination on the performance of the functionalized photoanodes and we provide insight into how the long-term stability is affected by ionomer degradation through isotopic labelling studies and FTIR measurements.

RESULTS AND DISCUSSION

Benchmarking the activity of bare photoanodes

Limited studies so far have reported the use of PEM-PEC reactors for gas phase water splitting[23-30], and a standardized method for evaluating the photoelectrochemical properties of photoanodes in this operation mode is still lacking. We therefore established an experimental protocol for benchmarking the activity of the photoanodes. In essence, photoelectrochemical activity was investigated under chopped UV-light irradiation during (a) PEM-PEC splitting of gaseous water sustained by humid air flow and (b) liquid water splitting in a conventional PEC cell, using the configurations shown in Figure 1. All performance tests were carried out in the range of T_{cell} = 30-70 ^{o}C, while the RH levels at the PEM-PEC cell were adjusted by varying the temperature of the gas saturator, T_{sat}.

For enabling PEM-PEC operation the photoanodes were interfaced to a polymer electrolyte. Two different commercial proton exchange polymer membranes were used, Nafion® and Aquivion®, both of them are perfluorinated sulfonic-acid membranes but having different side-chain lengths[33,34]. The membrane electrode assemblies (MEAs) were completed by a commercial Pt/C cathode and reference electrode.

According to a previously published work by our group, the specially designed PEM-PEC cell (Figure 1a) is equipped with a reference electrode which operates as a standard hydrogen electrode, enabling us to directly compare the performance of PEM-PEC and conventional PEC cells.

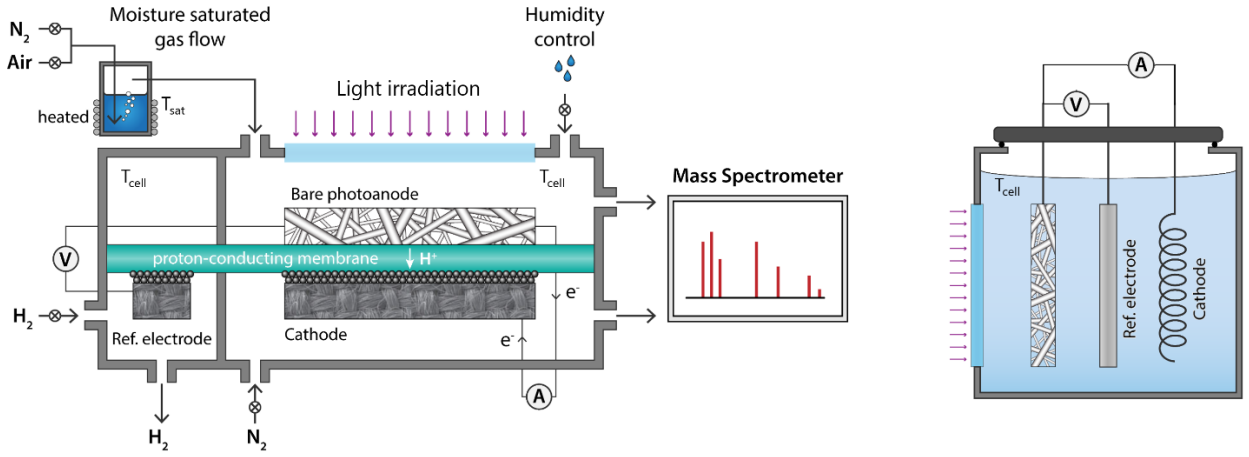

Figure 1. Experimental configurations used for evaluating the photoelectrochemical properties of photoanodes. (a) A PEM-PEC cell equipped with a standard hydrogen reference electrode, able to operate under humidified air flow with adjusted humidity levels. (b) A conventional PEC design.

Figure 2 gives a standardized format that we introduced for reporting photoelectrochemical activity of air-based operation of PEM-PEC cells. In essence, Figure 2 shows linear sweep voltammograms (LSV) obtained at 5 $mV \cdot s^{-1}$ using the bare Ti/TiO_2 photoanodes, when humidified air serves as the water feedstock in a PEM-PEC cell. Bare Ti/TiO_2 photoanodes are interfaced with Aquivion® and Nafion® (Figure 2a and 2b respectively) sheet membranes and the assemblies were evaluated with different levels of RH. Moreover, a comparison with liquid water operation in a conventional PEC cell is given in the same figure. The three electrode configuration was used in order to allow direct with conventional PEC literature (where a Pt coil[4,6-8] is commonly used as cathode and not Pt-GDE (gas diffusion electrode) as in our PEM-PEC cell). Due to the low overpotential of hydrogen evolution reaction the voltage between photoanode and cathode is not significantly different than the one between the photoanode and the reference electrode (Figure S1).

In all cases, anodic currents were obtained only upon irradiation. As illustrated in Figure 2, bare Ti/TiO_2 photoanodes exhibit high water oxidation activity only when RH reaches 200%. At 1.23 V, the photocurrent in humidified air operation at 200% RH reaches 0.57 $mA \cdot cm^{-2}$ with the Aquivion® membrane and 0.53 $mA \cdot cm^{-2}$ with the Nafion® membrane. These values correspond to 77% and 71% respectively of

the current obtained at the same potential in liquid PEC operation. This finding is in good agreement with literature[35] where it is reported that the photocatalytic water splitting reaction is critically dependent on the presence of a condensed water film on the semiconductor surface for proton conductivity from oxidation to reduction sites. Another interesting feature of Figure 2 is that the photoelectrochemical activity of the anode depends on the kind of polymer electrolyte used. The difference can be attributed to the different ionic conductivity of the membranes, which is also linked with water adsorption[33,34].

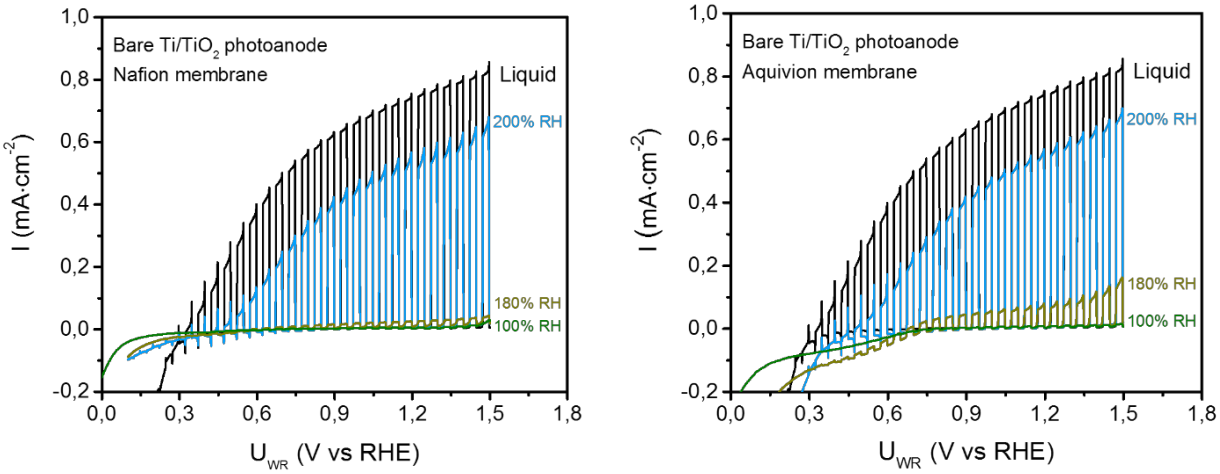

(a) (b)

Figure 2. LSV curves on the bare Ti/TiO_2 photoanodes under chopped illumination for water splitting in liquid PEC operation and in air-based PEM-PEC operation at various RH levels. In PEM-PEC investigations the membrane electrode assemblies were completed by (a) Nafion® polymer membrane (b) and Aquivion® polymer membrane.

Activity of functionalized Ti/TiO_2 photoanodes

Since air-sustained operation of PEM-PEC cells at RH below 100% cannot be realized with bare Ti/TiO_2 photoanodes (Figure 2a), functionalization is required aiming to improve water vapor capturing from the moisturized air flow and allow the formation of proton conduction channels across the photoanode. The strategy followed for photoanode functionalization is visualized in Figure 3 and is based on the impregnation of Aquivion® and Nafion® ionomer solutions[36-38] in the photoanodes.

Without a functionalized layer (Figure 3a) proton conduction across the fibers of the photoanode is not possible due to the lack of electrolyte medium. As shown later in this section, the applied ionomers cover the fibers of the porous photoanodes and gradually form a topcoat layer upon increasing the ionomer loading (Figure 3b). This coating has two functions, first, it provides a pathway for protons transfer from

the photoanode to the polymer membrane and second, it enables water adsorption from the humidity of ambient air (Figure 3b,c). H_2O absorbed in the ionomer and in the proximity of TiO_2 surface upon illumination reacts with photogenerated holes and drive O_2 evolution reaction. Protons are directed via the ionomer layer towards the membrane while electrons are conducted via the fibers towards the cathode where H_2 evolution is taking place. In Figure S2, there is further characterization (with SEM in the cross section of a fiber where the thicknesses of Ti core, TiO_2 and organic layers, identified by EDX are represented) which supports the graphical representation of the functionalized Ti/TiO_2 porous photoanode as well as the electrochemical impedance spectroscopy (EIS) data presented in next paragraph.

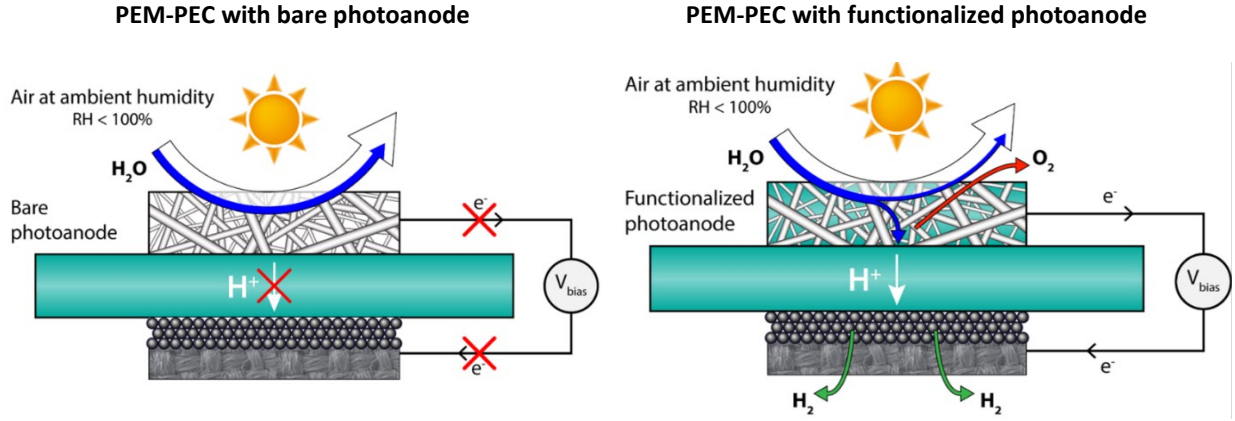

(a) (b)

PEM-PEC with functionalized photoanode: Close view on the interfaces developed upon functionalization

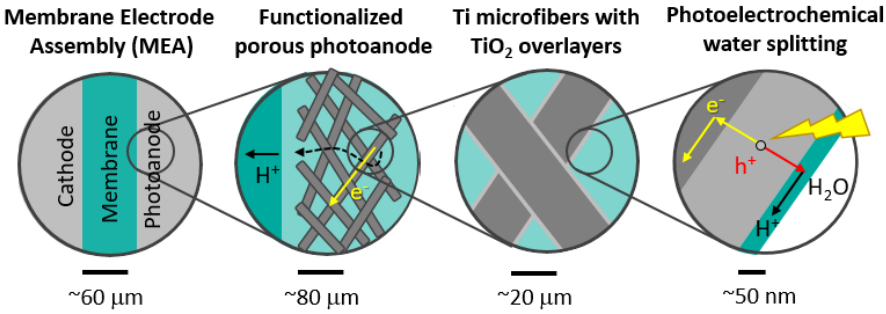

(c)

Figure 3. Schematic illustration of (a) air-based PEM-PEC operation using bare and (b) functionalized photoanodes at RH < 100 and (c) close view on the interfaces developed upon functionalization and pathways for proton conduction.

Figure 4 presents the Nyquist plots obtained with the bare and functionalized Ti/TiO_2 photoanodes during conventional liquid PEC water splitting (Figure 4a) and gas phase PEM-PEC operation at 100% RH (Figure 4b). For liquid PEC operation, similar impedance characteristics were obtained with bare and functionalized anodes, since water is available in the proximity of the photoelectrode via the electrolyte. This is not the case for the gas phase PEM-PEC operation, where a very different behavior is observed for the bare and functionalized photoanodes. Nyquist plots of the (Nafion® and Aquivion®) functionalized photoanodes are similar to those obtained in liquid PEC operation, in well alignment with the assumption that ionomer acts as channel for the proton transfer and water absorption medium. The shape of the Nyquist plot of the bare photoanode indicates that mass transfer limitations[39,40] play an important role in this system again in agreement with our assumption that without ionomer functionalization there is not enough water on the photoelectrode to allow the water oxidation and subsequent proton transfer to take place.

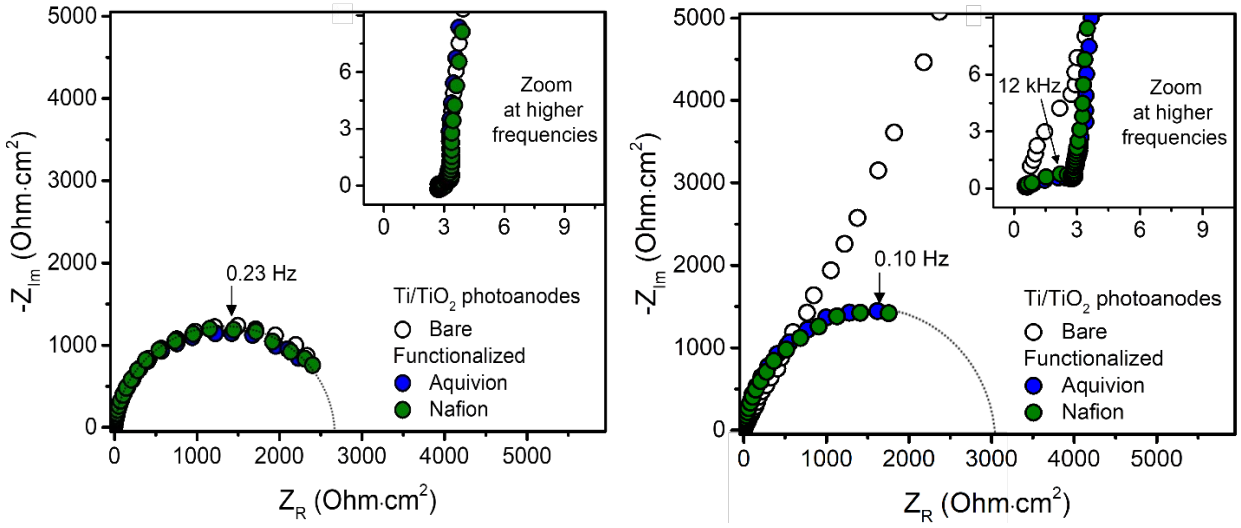

Figure 4: Nyquist plots (in two electrode, photoanode vs cathode -configuration) for bare and functionalized (10 mg·cm^{-2} Nafion® or Aquivion® ionomer loading) Ti/TiO_2 photoanodes at 1.23 V vs RHE and 10 mV amplitude in (a) conventional liquid PEC and (ii) PEM-PEC gas phase operation with 100% RH.

Overall, the EIS results are in line with the trend in photoelectrochemical activities of bare and functionalized photoanodes in liquid PEC and gas phase PEM-PEC operation (Figure 2). The intersect of the first semicircle with the horizontal axis, does not depend on the kind of photoanode used, indicating the electrolyte as the main contributor to ohmic losses. Overall ohmic resistance in the PEM-PEC configuration is lower than in the PEC (0.36 Ohm cm^2 and 2.7 Ohm.cm^2 respectively) due to the smaller

interelectrode distance[39,40]. The values of polarization resistance (determined by the difference between the high and low frequency intercepts of the anodic semicircle with the x-axis on the Nyquist plots) and the capacitance are also in qualitative agreement with the obtained photoelectrochemical activity of the various systems. The observed differences in the high frequency arcs (which corresponds to cathodic reaction, i.e. hydrogen evolution reaction) are attributed to the different cathodes utilized in each case i.e. Pt-coil in PEC vs Pt-GDE in PEM-PEC (see Figure 1).

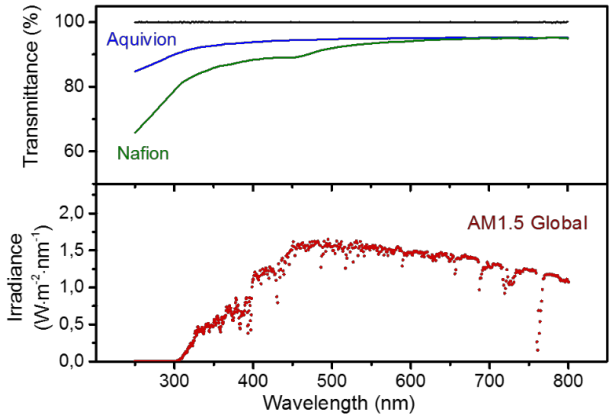

Figure 5. (Top) UV/Vis spectra of Nafion® and Aquivion® membranes, (bottom) standard solar spectra for AM 1.5 Global spectrum[28].

Even though both proton conducting polymeric membranes look transparent in the naked eye, we employed UV/Vis spectroscopy in order to investigate the exact levels of light adsorption as function of wavelength from 200 to 800 nm which is the area of interest for PEC applications. This quantification is important for the selection of coating for the functionalization of the photoanodes aiming for maximum ionomer transmittance. As shown in the transmittance spectra of Figure 5, Aquivion® shows, in general, higher light transmittance in comparison with Nafion®. For both materials the transmittance is high (>85%) in the visible light spectrum and thus the presence of the ionomers does not prevent the absorption of visible light at the photoanode. However, this is not the case for the UV region though, since Nafion® exhibits some capacitance for light absorption (transmittance drops to 79% at 300 nm). As we will see later in the manuscript, the proposed functionalization can be applied to various photoanodes so in the bottom part of the Figure 5 the AM 1.5 Global standard spectrum is given, for giving the reader an order of magnitude of the percentage of light loses that might occur. The levels of light transmittance correspond to 150 and 127 μm membranes, thus the actual levels of the shadowing effects of the coatings are smaller (see Figure S2). However, this information is very relevant in the case that one wants to use a

photoanode and a photocathode in each side of a polymeric membrane. In this case the light loses will be minor since the photoanode absorbs most of the high energetic photons of the solar spectrum.

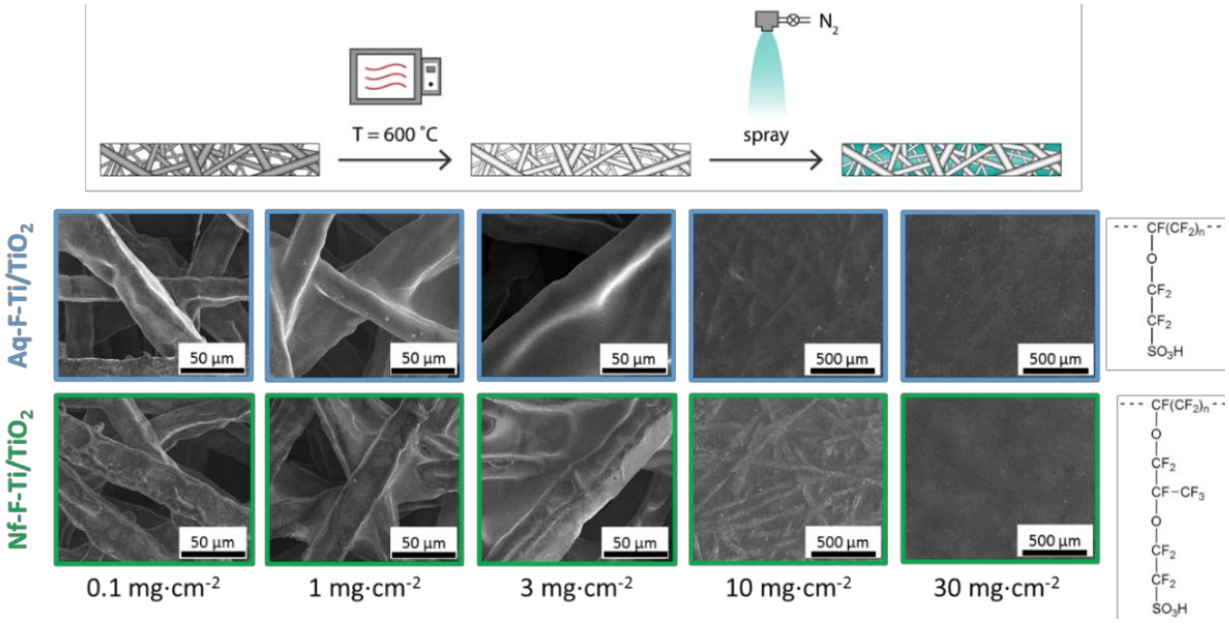

(a)

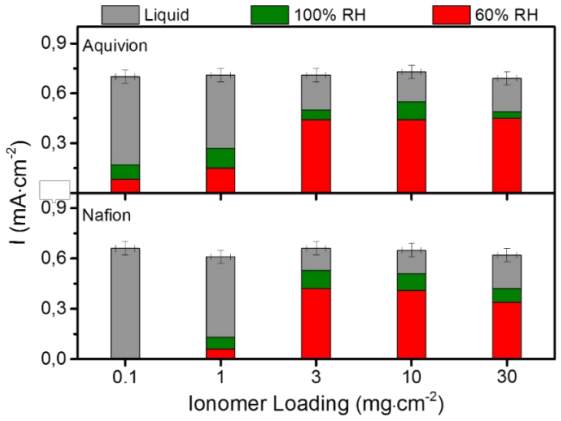

(b)

Figure 6. (a) SEM images of functionalized Ti/TiO_2 photoanodes using different ionomer loadings of Aquivion (top) and Nafion (bottom). (b) Photoelectrochemical activity at 1.23 V of functionalized Ti/TiO_2 anodes at liquid PEC operation and PEM-PEC air-based operation at 60% and 100% RH as a function of ionomer loading and kind of ionomer. Error bars represent standard errors.

As described in the experimental section, the Ti/TiO_2 photoanodes were developed via oxygen annealing of Ti porous substrates. Despite various the possibilities[22-24,41,42] we have chosen this fabrication method

due to its simplicity, reproducibility and uniformity. Figure 6a shows SEM micrographs of the functionalized photoanodes upon spray deposition of different amounts of Nafion® and Aquivion® ionomers. At 0.1 mg·cm^{-2} ionomer loading, only a small part of the photoanode is covered by ionomer. When ionomer loading reaches 3 mg·cm^{-2} a uniform top coating is observed on the photoanode fibers, while application of higher loadings leads to increase in the coating thickness. Extra SEM and optical microscopy images of the bare and functionalized photoanodes are also given in the supplementary information (Figure S2, S3).

The activity of the various functionalized Ti/TiO_2 photoanodes is summarized in Figure 6b, showing the effect of ionomer loading on the photocurrent density obtained under 1.23 V during air-operated PEM-PEC at 60% and 100% RH (the photocurrent at 0% RH is always zero) and during liquid PEC operation. After ionomer impregnation, photocurrents up to 0.5 mA·cm^{-2} were obtained at 60% RH, while bare photoanodes (without ionomer impregnation) are totally inactive (see also Figure 2). Overall, the results of Figure 6b show that indeed air-based PEM-PEC operation at 60% RH can be sustained using the functionalized photoanodes, demonstrating the success of the proposed strategy for the photoanode functionalization (Figure 3b,c).

Both with Nafion® and Aquivion® ionomers, increasing the ionomer content at the photoanode to higher photocurrents during gas phase PEM-PEC operation at 60% and 100% RH are obtained. Ionomer impregnation has small impact (within experimental error) on the photocurrent obtained during conventional liquid PEC operation. It has been reported in literature that Nafion ionomer coating of photoanodes can lead to increased photoelectrochemical activity as a result of accelerated charge transfer[20,28,35,43,44]. Our results provide evidence that ionomer loading (of Nafion or Aquivion) can also be used to efficiently capture water from ambient air.

With Aquivion® ionomer impregnation of small loadings (i.e. 0.1 mg·cm^{-2}) low photocurrents were obtained during air-based PEM-PEC operation, while this is not the case for Nafion® ionomer where loadings of at least 1 mg·cm^{-2} are required for functionalizing the photoanodes (Figure 6b). Under 60% RH, ionomer loadings of 3 mg·cm^{-2}and 10 mg·cm^{-2} show similar behavior (Figure 6b) having the highest photoelectrochemical activity for both kinds of ionomers. Further ionomer addition (i.e. 30 mg·cm^{-2}) causes drop in the performance, which can be attributed either on mass transfer limitations (extensive blocking of the pores) or on insufficient current collection (high electronic contact resistance between the photoanode and the bipolar plates of the PEM-PEC casing).

After this performance screening we decided to continue our studies with the 10 mg·cm^{-2} loading. The photoelectrochemical activity of the functionalized photoanodes with 10 mg·cm^{-2} ionomer loading is shown in detail in Figure 7. The main observations are that at 0% RH the photocurrent is negligible while for 60 and 100% a significant percentage of the performance vs liquid operation is recovered. In particular, 62% and 77% for Nafion® system while 60 and 73% for Aquivion® at 60 and 100% RH respectively at 1.23 V vs RHE.

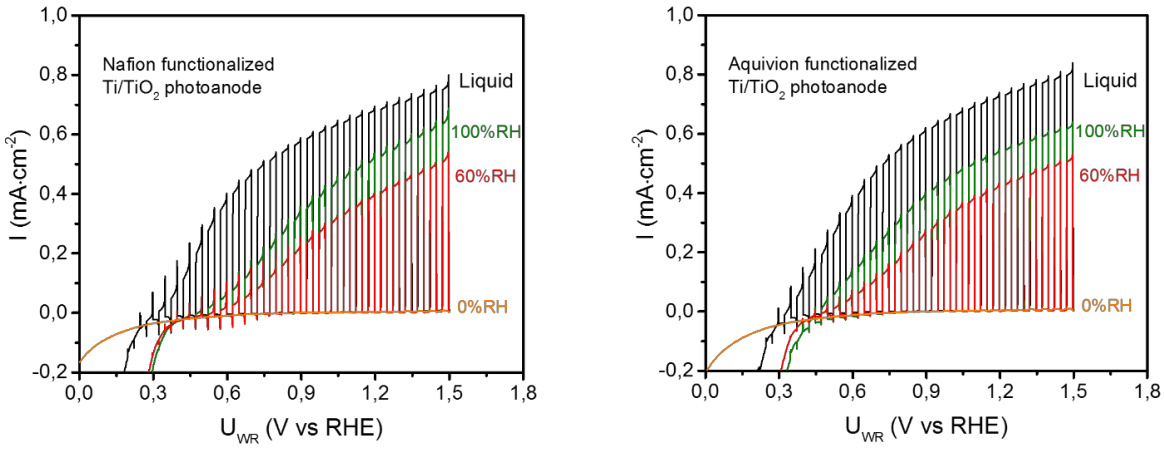

Figure 7. LSV curves at a scan rate of 5 mV/s under chopped illumination (LED-365 nm) during water splitting at the functionalized Ti/TiO_2 photoanodes. Each figure gives a comparison between liquid PEC operation and air-based PEM-PEC operation at various RH levels. Figures correspond to different ionomer types (with the same loading of 10 mg·cm^{-2}) and polymer membrane. Figures (a) correspond to Nafion® polymer membrane and ionomer and figure (b) to Aquivion® polymer membrane and ionomer.

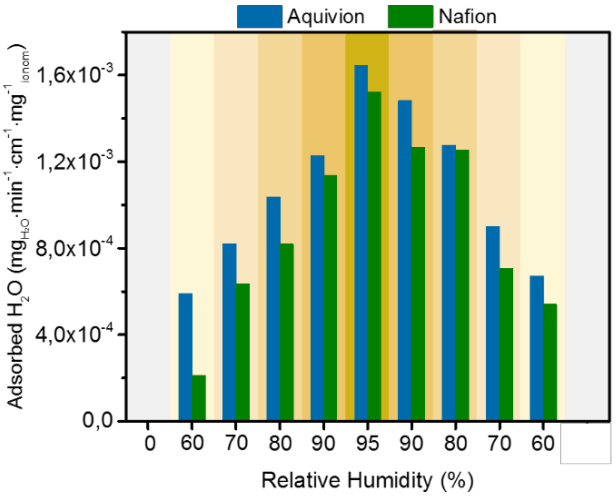

Figure 8: Water adsorption/desorption isotherms of the Aquivion® and Nafion® functionalized photoanodes.

To investigate whether this difference in behavior is related to different water absorbance, a detailed water sorption investigation was carried out by measuring the weight change of the functionalized photoanodes after ~120 min exposure to environments with different RH. As shown in Figure 8, within the examined RH range of 60%-95%, the photoanodes loaded with Aquivion® ionomer show larger water uptake from humidified air than Nafion®. The difference between the two kinds of ionomers is more pronounced at lower RH. Aquivion® containing photoanodes absorb 2.8 times larger amount of water at 60% RH compared to Nafion containing photoanodes. This ratio drops to only 1.1 at 95% RH. In addition, Nafion functionalized photoanodes desorb water faster than Aquivion®. Thus, results presented in Figure 6-8 demonstrate that in order to make hydrogen from ambient air, Aquivion® ionomer is more suitable for functionalizing agent compared to Nafion®.

Benchmarking stability of bare and functionalized Ti/TiO_2 photoanodes

The stability of the photoanodes was evaluated during gas phase PEM-PEC and conventional PEC water splitting using the experimental configurations of Figure 1. Stability tests were carried out at 30 ^oC and at thermodynamic potential (i.e. 1.23 V vs RHE). To resemble outdoor conditions, consecutive dark and illumination periods of 8 hours were applied, with a total duration for the stability test of 64 hours.

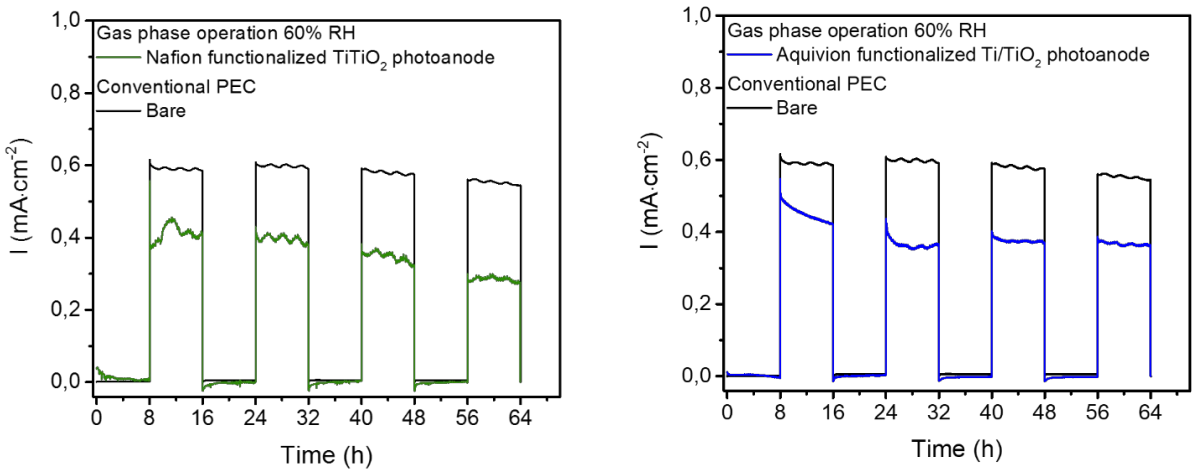

(a) (b)

Figure 9. Transient response of photocurrent during consecutive 8-hours periods of dark and illumination conditions. Black lines correspond to bare Ti/TiO_2 photoanodes during conventional liquid PEC water splitting. Green (a) and blue (b) lines correspond to air-based operation of PEM-PEC at 60% RH, using functionalized photoanodes with 10 mg cm^{-2} of Nafion and Aquivion ionomer, respectively.

Figure 9 gives a standardized format for reporting the durability of our photoanodes. The photocurrent profile during dark and illumination periods is shown for PEM-PEC operation at 60% RH with the Ti/TiO_2 photoanodes functionalized with 10 mg·cm^{-2} of Nafion® ionomer (blue line, Figure 8a) and Aquivion® ionomer (green line, Figure 8b). The incident photon to current conversion efficiency (IPCE) at the end of the first cycle is 13.2% for liquid operation and 9.38%, 9.60% for gas phase operation (at 60% RH) for Nafion® and Aquivion® respectively.

Our results demonstrate the high durability of Aquivion® functionalized photoanodes. After 4 dark-illumination cycles, the Nafion®-loaded photoanodes lost ~33% of their photoelectrochemical activity while the photocurrent of the Aquivion®-loaded photoanodes dropped by only 14% The photocurrent profile during the stability test protocol under conventional PEC operation with the bare Ti/TiO_2 photoanodes (black lines, Figure 9a and 9b) is also given for comparison. Bare photoanodes exhibited excellent stability, as evidenced by only ~8% drop in the photocurrent after 4 dark-illumination cycles.

The significant difference between the long-term stability of Nafion® and Aquivion® functionalized Ti/TiO_2 photoanodes can be attributed to various reasons, which can include the presence of side reactions or the degradation of the ionomer under prolonged irradiation. To gain further insights into the degradation mechanisms of functionalized photoanodes, a series of isotopic labelling and UV/Vis studies were carried out as described in the next section.

Mechanistic considerations

In order to further understand the mechanism and demonstrate the dynamic nature of this reaction, where water can be absorbed from the atmosphere and reacted to make hydrogen, isotopic labelling studies were carried out. For these experiments the photoanodes were supplied with air humidified with two different water isotopes, D_2O and $H^{18}O_2$, while the products at both compartments of the PEM-PEC cell were continuously monitored. The functionalized photoanodes with 10 mg·cm^{-2} of ionomer were used for these measurements.

Studies with D_2O (with 99.9% purity) and $H_2{}^{18}O$ (with 98.0% purity) aimed to define the faradaic efficiency of the process by measuring the products in the cathodic and anodic compartment respectively. In the isotopic labelled measurements, higher surface area photoanodes, in the order of 5 cm^2, were used to ensure higher photocurrents and thus higher signal to noise ratio in the product analysis.

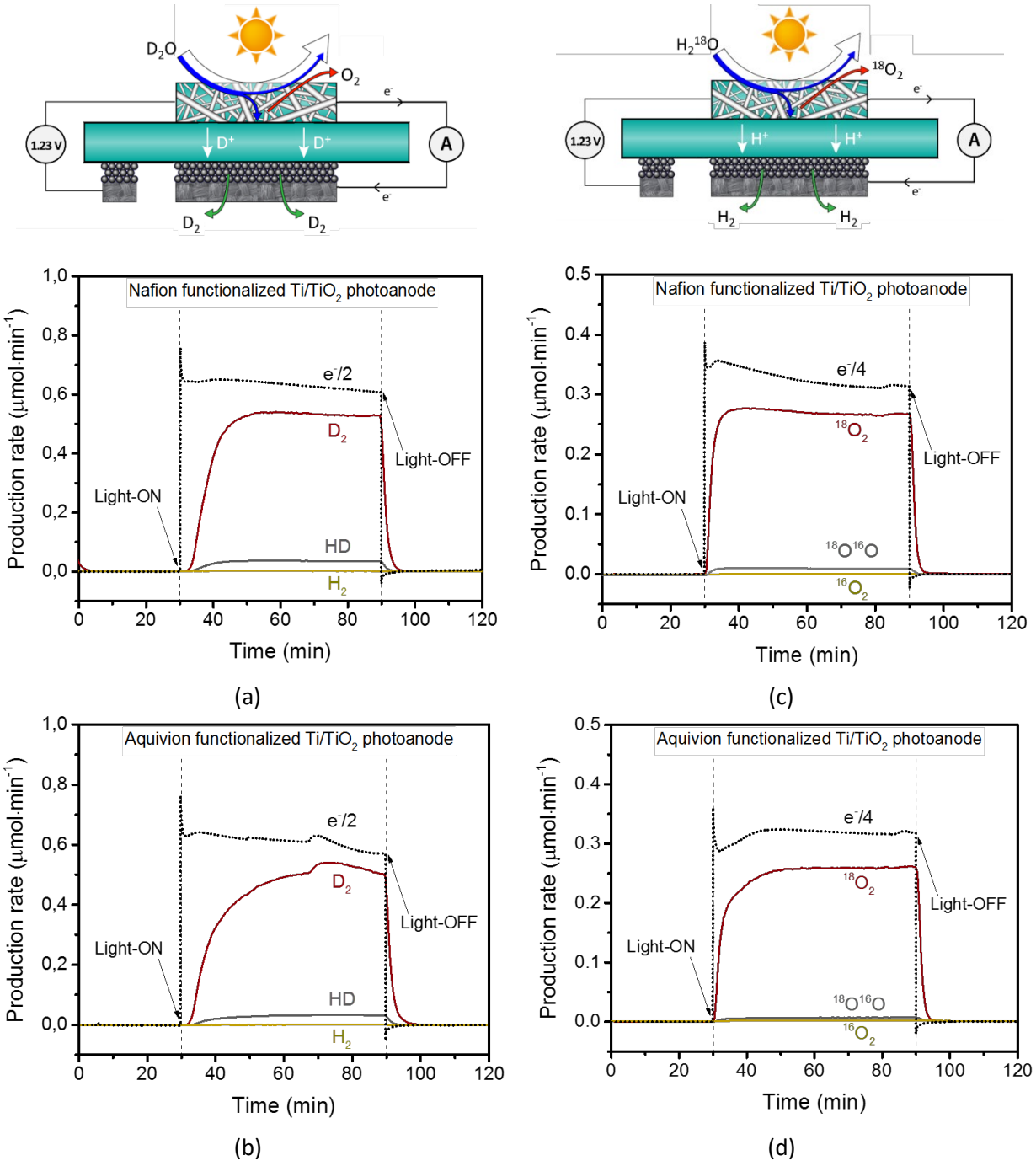

Figure 10. (a), (b) Faradaic rate (I/2F) and product distribution (H_2, HD and D_2) at the cathode of the PEM-PEC cell, while the photoanode is supplied with D_2O-humidified air at 80% RH. (c), (d) Faradaic rate (I/4F) and product distribution ($^{18}O_2$, $^{16}O^{18}O$ and $^{16}O_2$) at the photoanode of the PEM-PEC cell, while it is supplied with $H_2{}^{18}O$-humidified air at 80% RH. Operation occurred at a comparable photocurrent in the region of 2 mA. Illumination periods are indicated. Ti/TiO_2 photoanodes were used functionalized with 10 $mg \cdot cm^{-2}$ of Nafion® and Aquivion® ionomer.

Figure 10a,b show the product distribution at the cathode compartment of the PEM-PEC cell upon illumination of the functionalized photoanode which is supplied with air humidified with deuterated water. D_2 is the main detected product, while small concentrations of HD were also detected. Similarly, Figure 9c,d show the product distribution at the photoanode compartment of the PEM-PEC cell for the case of operation under air humidified with $H^{18}O_2$. In these cases, $^{18}O_2$ is the main detected product at the photoanode side, while traces of $^{18}O^{16}O$ were detected as well. The existence of HD and $^{18}O^{16}O$ (Figure 10) in the products of the cathode and photoanode compartment respectively is probably related to residual H_2O and H^+ attached in the sulfonated group of the ionomer or polymeric membrane. The hydrogen faradaic efficiency (with this term we also include any combination of H and D atoms) from the D_2O experiments was estimated at ~90% for both Aquivion® and Nafion® functionalized photoanodes, which is in good agreement with the literature[18,20].

The oxygen faradaic efficiency estimated from the $H^{18}O_2$ experiments was slightly lower, at ~84% for Aquivion® and ~87% for Nafion® functionalized photoanodes also in good agreement with literature[18,20]. Overall, faradaic efficiencies for oxygen and hydrogen are similar for both kinds of functionalized photoanodes and are high enough to confirm that photoelectrochemical water splitting takes place and parasitic reactions, if any, take place at a low extent. The lower values of the faradaic efficiency for the oxygen evolution reaction suggest that a part of the oxygen generated could be used in other oxidation processes.

Factors determining the durability of functionalized Ti/TiO_2 photoanodes

In order to assess if parasitic reactions take place and whether they affect the durability of the functionalized photoanodes, further isotopic labelling studies were carried out. In order to identify possible degradation pathways, the MS signals for CO_2 isotopes were followed while monitoring the product distribution at the compartment of the photoanode, which operates under air humidified with $H^{18}O_2$. Nafion degradation during PEC operation has been reported in recent literature [18,20,43,44] however, to the best of our knowledge, there is no literature available on Aquivion degradation under UV light.

The corresponding results are given in Figure 11, showing that CO_2 is produced at both photoanodes, mainly as $C^{16}O_2$. Since the ionomer is the only C-containing phase at the photoanode, a very likely explanation is that the side reaction responsible for CO_2 formation is the photoelectrochemical oxidation of the ionomers. Interestingly from Figure 11 it appears that the overall CO_2 production is ~2 times higher for the Nafion® functionalized photoanode than Aquivion®, showing that Nafion ionomer is less stable than Aquivion®. This finding is qualitatively in-line with the lowest durability of the Nafion®-functionalized

Ti/TiO_2 photoanodes (Figure 9). However, the ionomer photoelectrooxidation is not the single reason that affects the durability of functionalized photoanodes, as we will see in the next paragraph the degradation of the polymeric membranes upon UV irradiation is the second one.

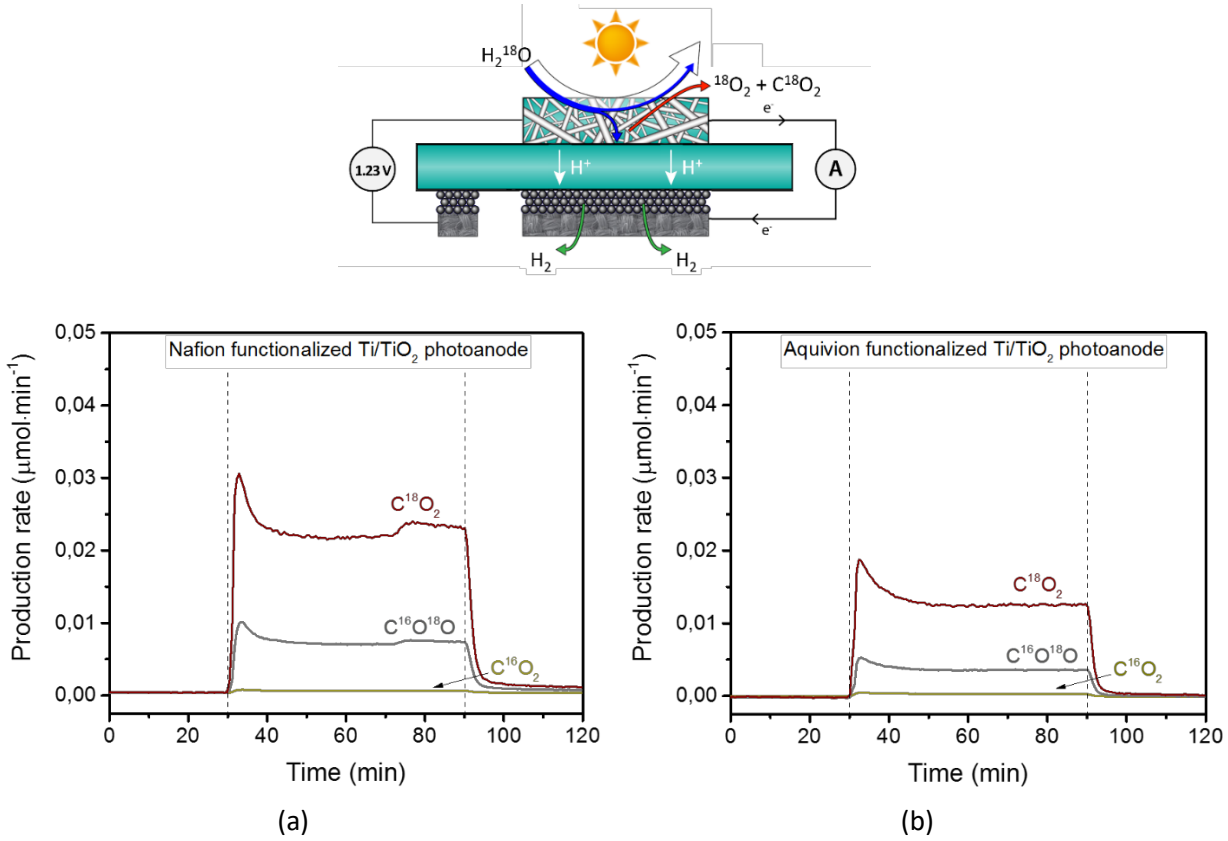

Figure 11. Photocurrent (top panel) and CO_2 isotope distribution (bottom panel) at the photoanode of the PEM-PEC cell, which is supplied with $H_2{}^{18}O$-humidified air at 80% RH and operated under 1.23 V vs RHE. Operation occurred at a comparable photocurrent in the region of 2 mA. Illumination periods are indicated. Ti/TiO_2 photoanodes were used functionalized with 10 mg cm^{-2} of (a) Nafion® ionomer and (b) Aquivion® ionomer.

It is known that exposure to UV radiation can cause degradation of many polymers, resulting to breaking of polymer chains, production of free radicals and reduction of the molecular weight[45,46]. To investigate the stability of Aquivion® and Nafion® polymers during prolonged exposure to UV irradiation (LED-365 nm), UV-Vis spectroscopy was used. As shown in Figure 12, the light transmittance for Nafion® is heavily affected after 16 h or UV irradiation and a significant drop in the light transmittance, which becomes negligible for wavelengths below 300 nm. Aquivion® on the other hand remains stable even after its 40 hours exposure to UV irradiation.

A general conclusion drawn on the basis of Figures 10-12, is that Aquivion® is the most appropriate and durable agent for functionalizing Ti/TiO_2 photoanodes, since Nafion® is more vulnerable to both photoelectrochemical oxidation and also to structural degradation during long-term testing under UV irradiation. The extent at which each of these degradation mechanisms affect the stability of Nafion® functionalized Ti/TiO_2 photoanodes is yet unclear from the present experimental results, but is worth for further investigation. Moreover, the UV/Vis spectra of Figure 12 indicate no changes in the visible light transmittance of both polymers. It can be thus expected that both ionomers can be effectively used for functionalization of visible-light active photoanodes. Even if transmittance is hindered at the UV region the visible part of the solar spectrum can be utilized by visible light absorbers.

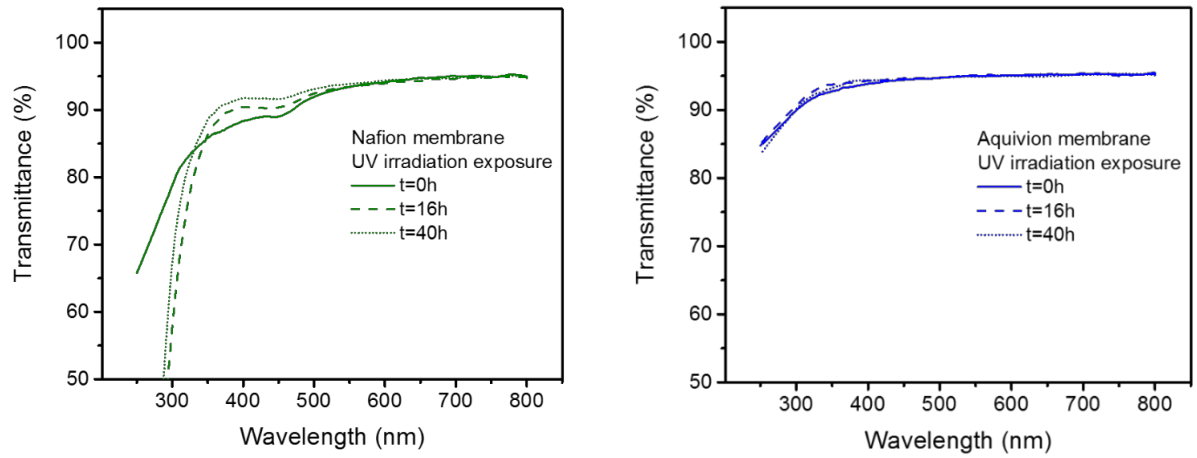

(a) (b)

Figure 12. UV-Vis spectra of (a) Nafion® and (b) Aquivion® membranes after different times of exposure to UV irradiation (LED - 365 nm).

In order to verify the generality of the concept and to confirm the assumption that performance degradation is happening due to UV degradation, a new class of Aquivion and Nafion functionalized photoanodes was developed, able to operate in the visible spectrum of the light, and their performance and durability was compared, as shown in the next section.

Activity and stability of functionalized W/WO_3 photoanodes

Aiming to verify if the kind of ionomer plays a role on the stability of visible-light active photoanodes, we developed a series of functionalized W/WO_3 photoanodes and carried out a systematic investigation on their photoelectrochemical properties under visible light illumination (LED 415 nm). Similarly to the Ti/TiO_2 case, the W/WO_3 photoanodes were developed after annealing a porous W substrate. Due to

structural differences between the two substrates, the W/WO_3 photoanodes possess a more open structure and wider fiber diameter (Figure 13) compared to Ti/TiO_2 photoanodes (Figure 6a). In order to ensure a similar ionomer coating thickness on the both W/WO_3 and Ti/TiO_2 photoanodes, a 3 $mg \cdot cm^{-2}$ Aquivion® and Nafion® loading was applied in the W/WO_3 case. Cross-sectional SEM images of the functionalized anodes are also given in the supplementary information (Figure S4).

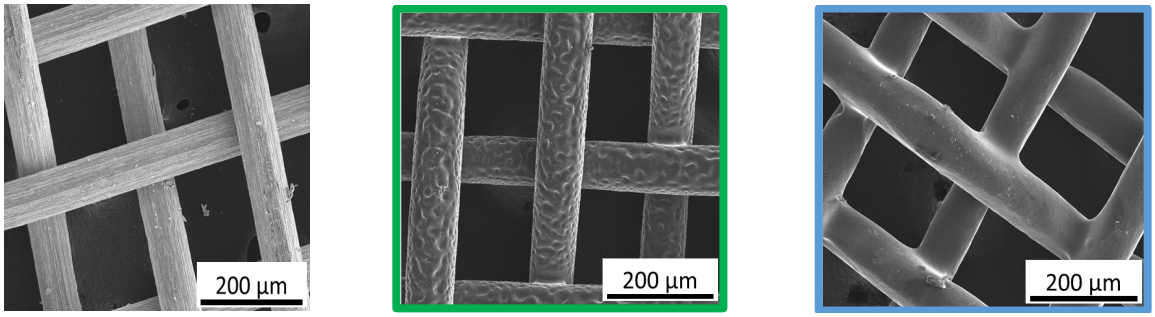

(a) (b) (c)

Figure 13. SEM images of the W/WO_3 photoanodes: (a) bare, (b) functionalized with Nafion®, (c) functionalized with Aquivion®. Ionomer loading: 3 $mg \cdot cm^{-2}$.

Figure 14 shows linear sweep voltammograms obtained with the functionalized W/WO_3 photoanodes in air-based PEM-PEC cell at various RH levels and in liquid PEC operation, under chopped light illumination. Functionalised W/WO_3 photoanodes with Aquivion® or Nafion® exhibited excellent activity since at 1.23 V vs RHE and 60% RH were able to recover up to 84% and 81% of the performance obtained with liquid water (i.e. conventional PEC operation) respectively. More importantly, at higher potential values the recovery is very close to 100%. The level of recovery (air-based at 60 % RH vs liquid operation) was found to be higher for the functionalized W/WO_3 photoanodes (~84 %) compared to the Ti/TiO_2 ones (~62 %). This is very likely to be related with the different open area and microstructure between the two types of photoanodes which results in different ionomer coatings. In Ti/TiO_2 a thick coating is created on the top of the photoanode and a thin layer around the rest of the fibers, while for the case of W/WO_3 a thick coating is deposited around the fibers (Figure S2, S4). As a results different charge transfer, light and water management are taking place.

This assumption was also validated by comparing the photoelectrochemical activity of Ti/TiO_2 photoanodes (Figure S5) with (i) the same porosity (80%) and different thickness (0.4 and 0.2 mm) and (ii) same thickness (0.4 mm) and different porosity (50 and 80%). Indeed, decreasing the thickness of the photoanode for constant porosity increases the performance, while decreasing the porosity for constant

photoanode thickness lowers the performance. A detailed analysis on the effect of microstructure on photoelectrochemical performance will be the topic of an upcoming article by our group.

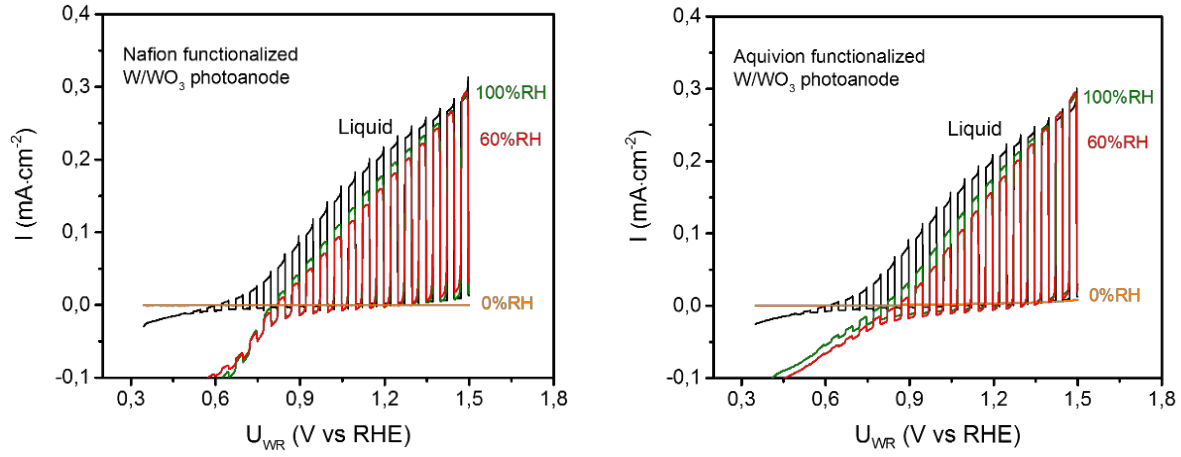

(a) (b)

Figure 14. LSV curves at a scan rate of 5 $mV \cdot s^{-1}$ under chopped light illumination (LED - 415 nm) during water splitting at the functionalized W/WO_3 photoanodes with (a) Nafion® and (b) Aquivion®. Each figure gives a comparison between liquid PEC operation and air-based PEM-PEC operation at various RH levels. Ionomer loading: 3 $mg \cdot cm^{-2}$.

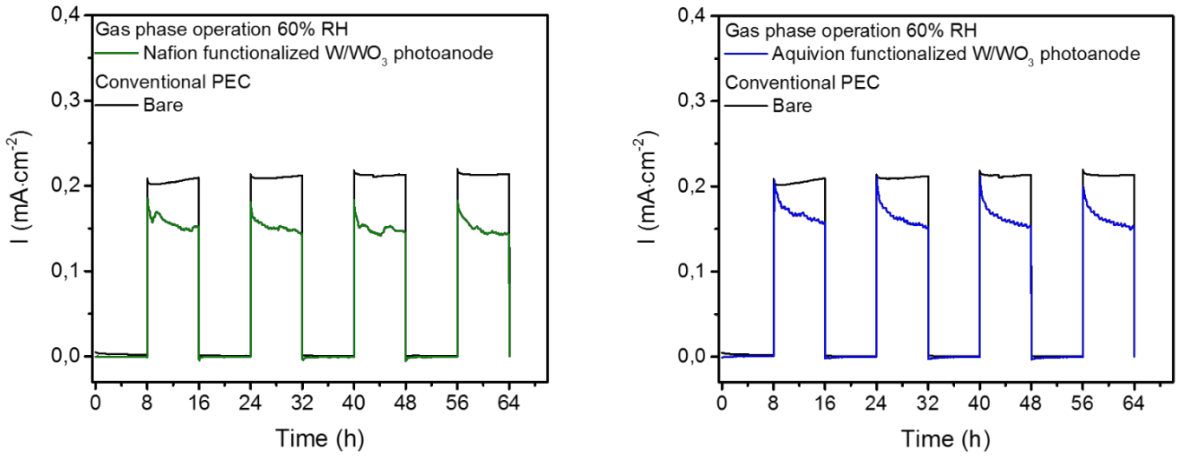

(a) (b)

Figure 15. Transient response of photocurrent during consecutive 8-hours periods of dark and illumination (LED-415nm) conditions at the functionalized W/WO_3 photoanodes with (a) Nafion® and (b) Aquivion®, during air-based PEM-PEC operation at 60% RH and conventional liquid PEC water splitting. Ionomer loading: 3 $mg \cdot cm^{-2}$.

The durability of Aquivion® and Nafion® functionalized W/WO_3 photoanodes is depicted in Figures 15. The IPCE at the end of the first cycle is 2.16% for liquid operation and 1.56%, 1.61% for gas phase operation (at 60% RH) for Nafion® and Aquivion® respectively. In-line with the UV-Vis investigations (Figure 13)

which suggest long-term stability in the visible light transmittance of Aquivion® and Nafion®, both photoanodes showed only slight deactivation after the 64-hours stability testing protocol. Specifically, both kinds of photoanodes showed a ~2.5% deactivation after 4 consecutive dark-light cycles in air-based PEM-PEC operation at 60%. UV/Vis and isotopically labelled studies similar to the previous section were also conducted for this class of photoanodes. In line with the durability studies there was any noticeable modification in the light transmittance (Figure S6) and the CO_2 emissions were below our detection limit.

Expanding operating conditions

Our data provide strong evidence that the proposed photoelectrode functionalization could be the basis for future self-standing PEC installations in remote areas, which means that we need to expand our operating conditions to include more geographical areas (Figure S7). In order to evaluate the performance recovery when operating at higher cell temperatures and lower humidity we have performed experiments at 50 and 70 ^{o}C PEM-PEC cell temperature for RH 0, 30, 60, 100%.

The photoelectrochemical activity of the Aquivion® functionalized photoanodes (with 10 and 3 mg·cm^{-2} ionomer loading for Ti/TiO_2 and W/WO_3 photoanodes) is shown in detail in Figure 16. The main observations are that at 0% RH the photocurrent is negligible while for 30, 60 and 100% a significant percentage of the performance vs liquid operation is recovered at 1.23 V vs RHE (while full recovery is obtained at higher potentials). In the following table is presented the photocurrent recovery of the two classes of Aquivion® functionalized photoanodes at all the sets of operating conditions.

Table -1: Comparison of the gas phase PEM-PEC operation vs the conventional liquid

Tcell (^{o}C)	RH (%)	Photocurrent recovered in gas phase vs liquid operation at 1.23 V vs RHE	
		Aquivion® functionalized Ti/TiO_2 photoanodes	Aquivion® functionalized W/WO_3 photoanodes
30	60	60	84
30	100	73	91
50	30	32	17
50	60	60	90
50	100	64	92
70	30	8	11
70	60	62	75
70	100	67	88

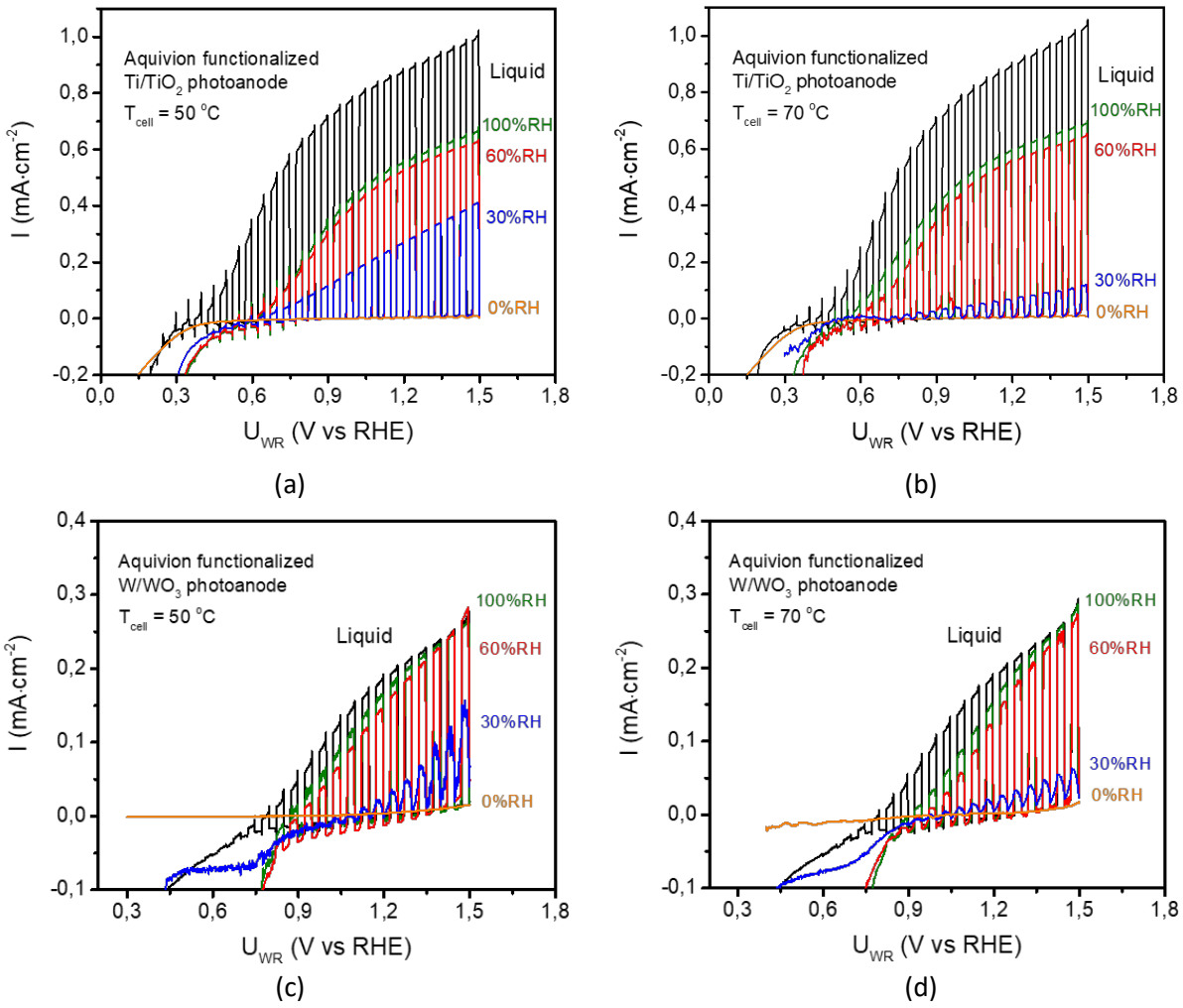

Figure 16. LSV curves at a scan rate of 5 $mV \cdot s^{-1}$ under chopped light illumination during water splitting at the Aquivion® functionalized (a),(b) Ti/TiO_2 photoanodes and (c), (d) W/WO_3 photoanodes at 50 and 70 ^oC respectively. Each figure gives a comparison between liquid PEC and air-based PEM-PEC operation at various RH levels. Ionomer loading: 10 and 3 $mg \cdot cm^{-2}$ for Ti/TiO_2 and W/WO_3 photoanodes respectively.

The photoelectrochemical activity of the Aquivion® functionalized photoanodes (with 10 and 3 $mg \cdot cm^{-2}$ ionomer loading for Ti/TiO_2 and W/WO_3 photoanodes) is shown in detail in Figure 16. The main observations are that at 0% RH the photocurrent is negligible while for 30, 60 and 100% a significant percentage of the performance vs liquid operation is recovered at 1.23 V vs RHE (while full recovery is obtained at higher potentials). In the following table is presented the photocurrent recovery of the two classes of Aquivion® functionalized photoanodes at all the sets of operating conditions.

CONCLUSIONS

The photoelectrochemical properties of ionomer-functionalized, porous Ti/TiO2 and W/WO3 photoanodes, were evaluated for vapor-phase water-splitting in a PEM-PEC cell. Photoanode functionalization was achieved by the impregnation of the porous photoanodes by two different commercial perfluorosulfonic acid ionomers, Nafion® (DuPont) and Aquivion® (Solvay). While bare photoanodes are inactive in air-based PEM-PEC operation at 60% RH, functionalized photoanodes were able to recover up to 90% of the performance obtained at 1.23 V of the performance in liquid operation. The activity is attributed to (i) the creation of prolonged ion transport channels and (ii) the uptake of humidity from ambient air by the ionomers, with Aquivion exhibiting a higher water absorption capacity. Our results suggest that the porosity and the open area of the photoelectrodes have significant effect on the performance recovery.

Both Nafion® and Aquivion® functionalized photoanodes showed excellent stability over 64 hours visible light - dark cycling. However, Nafion® undergoes degradation under UV-irradiation whereas Aquivion® was found to exhibit high stability. The extent to which this degradation affects the stability of Nafion® functionalized photoanodes is not yet clear and warrants further investigation.

EXPERIMENTAL METHODS

Photoelectrode preparation

Three different commercially available Ti-felts with a web of microfibers were used in this study. The main experimental course, though, was carried out with a Ti-felt with the following geometrical characteristics; 0.4 mm felt thickness, 20 μm wire thickness, 80% porosity, Bekaert. The other two Ti-felts had differences concerning the porosity (i.e. 50% and 80%) and the felt thickness (i.e. 0.4 and 0.2 mm). On the other hand, the W-mesh (100 mesh, 0.12 mm mesh thickness,60 μm wire thickness, 36% open area) was purchased from Werson industrial group. Prior to the O_2 annealing procedure, the samples underwent a cleaning process using acetone and ethanol for 20 minutes respectively in a sonic bath. Then, the samples were rinsed with deionized water and dried under air flow in room temperature. The Ti and W samples were annealed at 600^{o}C for 2 h and 550 ^{o}C for 5 h respectively under air atmosphere in order to grow a thick and crystalline oxide layer around the microfibers.

Photoelectrode functionalization

The functionalization of the photoanodes includes the deposition of multiple loadings, of Nafion® (5 wt.%, Sigma-Aldrich) and Aquivion® (D72-25DS, 25 wt.%, Sigma Aldrich) ionomers in the region of 0-30 $mg \cdot cm^{-2}$. The ionomer precursors were synthesized after 4 mL of Nafion® and 1mL of Aquivion® were diluted in 20 mL of ethanol in order to reduce the viscosity of the solution. The ionomers were deposited while the photoanodes were on a hotplate (60 ^{o}C) using the spray coating/deposition technique. The gravity feed spray coater was connected with air flow supply of 10 $mL \cdot min^{-1}$. Sample to nozzle distance was 10 cm. The spray protocol was consisted of ~10 s spray time per 9 cm^2 of photoelectrodes surface area followed by an idle time of ~10s. 1 spray cycle includes 5 vertical line coatings and 5 horizontal ones. The functionalized photoelectrodes had geometrical surface area of 9 cm^{-2}, unless stated otherwise, and were kept overnight in a drying oven after deposition (60 ^{o}C) to facilitate ethanol and water evaporation.

Physicochemical characterization

The surface and structure morphologies of the photoanodes before and after ionomer application were characterized by a FEI Quanda 3D FEG Instrument and a TESCAN VEGA3 scanning electron microscope (SEM). The crystal phases of the unmodified and the O_2 annealed samples were analysed in a X-ray diffractometer (Brucker D8 Advance Eco) using a Cu K_α tube (Figure S8). Finally, the diffuse reflectance and the transmission of the O_2 annealed photoanode and the membranes respectively were measured in a Perkin Elmer 1050 UV-Vis and IR spectrophotometer in the integrating sphere setup configuration, between 250 and 800 nm (Figure S9).

Photoelectrochemical characterization

The photoelectrochemical properties of the photoanodes in gas and liquid phase operation were studied in an electrochemical work station supplied by Ivium (Vertex). Chopped light Linear Sweep Voltammetry (LSV) measurements, in a scan rate of 5 $mV \cdot s^{-1}$, and transient chronoamperometric measurements were performed under UV irradiation (M365P1, 365 ± 15 nm, ThorLabs, 15 $mW \cdot cm^{-2}$) for when Ti/TiO_2 photoanodes were utilized and under visible light irradiation in case of W/WO_3 photoanodes (M415LP1, 415 ± 14 nm, 29 $mW \cdot cm^{-2}$). The illuminated geometrical surface area was 1 cm^{-2}. The photoelectrochemical performance of the Ti/TiO_2 and W/WO_3 photoanodes was evaluated under UV LED (M365P1) and vis-LED (M415LP1) light illumination, while for comparison reasons, LSV measurements of the same bare photoanodes were conducted under AM 1.5 class A solar simulator (LCS 100, Oriel Instruments) using a 100 W Xe lamp with a calibrated illumination intensity of 80 $mW \cdot cm^{-2}$ at the sample position (Figure S10).

The cathode was comprised by Pt particles deposited on a carbon cloth (FuelCellsEtc, 0.5 mg·cm^{-2}, 4 or 9 cm^2). The same material was used as reference electrode (0.5 cm^{-2}) for gas phase operation experiments. The different relative humidity (RH) levels (*i.e.* 0, 30, 60, 100%) in gas phase operation were obtained as the temperature of the saturator was adjusted between 22 to 43 ^{o}C while the cell's temperature remained stable at 30, 50, 70 ^{o}C. The RH levels were monitored by a temperature-humidity recorder (P750, Dostmann electronic GmBH). For 0% RH measurements the saturator was bypassed and in order to avoid water vapor enrichment of the gas stream. At the same time gas lines were heated at 70, 90 ^{o}C in order to avoid water condensation in the lines. Table S1 summarizes the temperature conditions of the saturator to obtain different RH levels. Prior to electrode evaluation, the system was idle for 20 min under the water vapor stream to elaborate the water absorbance from the ionomer.

The incident photon-to-current conversion efficiency (IPCE) was calculated using the following equation.

$$ICPE = (I_{ph} \cdot 1240/\lambda)/I_o$$

I_{ph} is the steady state photocurrent density (mA·cm^{-2}), 1240/λ is the photon energy (eV) at a certain wavelength and Io in the power of the monochromatic light source (mW·cm^{-2})

PEM-PEC cell operation

Two different polymeric electrolyte membrane types were used in the gas phase operation experiments, the Nafion® perfluorinated membrane (127 μm thick, FuelCellsEtc) and the Aquivion® membrane (150 μm thick, E98-15S, Sigma-Aldrich). After the functionalization, the Ti-felt photoanode was placed on top of the appropriate membrane, while the Pt/C cathode was placed on the bottom side. The third electrode of our cell, which represents the reference electrode was also a Pt/C electrode. The design of our custom made PEM-PEC cell is also depicted and described in our previous work[22,24]. Impedance spectroscopy has been used to determine the cell resistance and 80% iR correction has been applied for the LSV results.

During the experimental mode, air stream of 50 mL·min^{-1} was saturated with water vapor in a thermostated water saturator (or by passed when 0% RH was the target) and reached the surface of the photoanode through thermostated gas lines. The temperature of the cell was varied from 30-70 ^{o}C and in order to achieve the relative humidity levels between 30 and 100% the temperature of the saturator was increased from 22 to 70 ^{o}C respectively (see Table S1). He gas flow of 50 mL·min^{-1}, which was not enriched with water, was purged in the cathodic compartment, while H_2 flow in the reference electrode compartment was 30 mL·min^{-1}.

Conventional PEC cell operation

A three electrode conventional PEC cell was used for the conduction of electrochemical tests in aqueous electrolyte at pH=1 (0.1 M H_2SO_4). The cell was consisted from a Pt wire as cathode (Sigma-Aldrich) and a Ag/AgCl reference electrode (RE-1S, ALS Japan). The applied potential between the photoanode and the reference electrode was converted to the reverse hydrogen electrode (RHE) scale using the Nernst equation.

$$E_{(\mathrm{RHE})} = E_{(\mathrm{Ag/AgCl})} + 0.059\ \mathrm{pH} + 0.197$$

Impedance spectroscopy has been used to determine the cell resistance and 80% iR correction has been applied for the LSV results.

Isotopic labelling experiments

The experiments with isotopic labelled water species were performed in different setup parameters. In detail, H_2O was replaced in the thermostated saturator with deuterium oxide (D_2O, 99.9 atom%, Sigma-Aldrich) and ^{18}O enriched water ($H_2{}^{18}O$, 98.06%, Isoflex) for D_2 and $^{18}O_2$ qualitative measurements in the cathodic and anodic compartment respectively. The D_2 and $^{18}O_2$ levels were determined by a Hiden QGA quadrupole mass spectrometer (MS) operating in selected ion mode with a SEM detector. The carrier gasses were also substituted; air was substituted by N_2 while He was substituted by Ar in order to avoid misleading measurements, as He has the same mass with D_2 and $^{16}O_2$ could be a by-product of the process. In addition, in order to overcome the MS detection limit of hydrogen and oxygen species, the geometrical (photo)electrode active surface area was increased (5 cm^2). In that case a high surface area UV lamp, comprised of 9 LED lamps, was utilized (Opsytec Dr. Groebel,). The setup scheme is depicted in Figure. 1.

ASSOCIATED CONTENT

Overpotential analysis. SEM and optical micrographs of the functionalized photoanodes (cross section and EDX analysis). Performance evaluation of Ti/TiO_2 with different microstructural characteristics. UV/Vis spectra for Nafion membrane. Weather data. XRD patterns and UV-Vis absorption spectra of bare Ti/TiO_2 and W/WO_3. Bare photoanode performance under one sun illumination. Table with gas saturators temperature for achieving various RH levels.

AUTHOR INFORMATION

Corresponding Author: Mihalis N. Tsampas.

Email m.tsampas@differ.nl , Phone +31403334820

The authors declare no competing financial interest.

ACKNOWLEDGMENTS

This work is part of the program 'CO2-neutral fuels' Grant No. 700.001.516.50, of NWO-I, formerly known as the Foundation for Fundamental Research on Matter (FOM), which is financially supported by the Netherlands Organisation for Scientific Research (NWO) and Shell Global Solutions International B.V. This research program is co-financed by Toyota Motor Europe. We would like to thank E. Langereis (DIFFER) for the illustrations, I. Schreur-Piet (TU.e) and, Christiaan van Roost and Horst Heinrichs (AGFA) for the assisting in the functionalized photoanode characterization.

TABLE OF CONTENT (GRAPHICAL ABSTRACT)

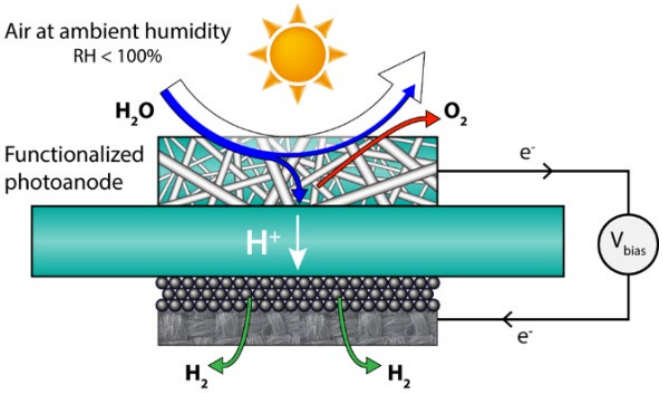

REFERENCES

[1] van de Krol, R.; Gratzel, M. (Eds.), Photoelectrochemical Hydrogen Production, Springer, New York, 2012.

[2] BP Statistical Review of World Energy 2018, BP plc, p.9, 2018.

[3] McGlade, C.; Ekins, P. The Geographical Distribution of Fossil Fuels Unused when Limiting Global Warming to 2 °C, Nature 2015, 517, 187–190.

[4] Lewerenz, H. J.; Peter, L. (Eds.) Photoelectrochemical Water Splitting: Materials, Processes and Architectures, RSC publishing, Cambridge, U. K. 2014.

[5] Lewis, N. S.; Nocera, D. G. Powering the Planet: Chemical Challenges in Solar Energy Utilization, PNAS 2006, 103 (43), 15729-15735.

[6] Sivula, K.; van de Krol, R. Semiconducting Materials for Photoelectrochemical Energy Conversion, Nat. Rev. Mater. 2016, 1 (2), 15010 (1-17).

[7] Lee, D. K.; Lee, D.; Lumley, M. A.; Choi, K. S. Progress on Ternary Oxide-based Photoanodes for Use in Photoelectrochemical Cells for Solar Water Splitting, Chem. Soc. Rev. 2019, 48, 2126-2157.

[8] Chen, Z.; Dinh, H. N.; Miller, E. Photoelectrochemical Water Splitting Standards, Experimental Methods and Protocols, Springer, New York, 2013.

[9] Cheng, W. H.; Richter, M. H.; May, M. M.; Ohlmann, J.; Lackner, D.; Dimroth, F.; Hannappel, T.; Atwater, H. A.; Lewerenz, H. J. Monolithic Photoelectrochemical Device for Direct Water Splitting with 19% Efficiency, ACS Energy Lett. 2018, 3, 1795-1800.

[10] Young, J. L.; Steiner, M. A.; Döscher, H.; France, R. M.; Turner, J. A.; Deutsch, T. G.; Direct Solar-To-Hydrogen Conversion via Inverted Metamorphic Multi-Junction Semiconductor Architectures, Nat. 2017, 2, 17028.

[11] MacLeod, B. A.; Xerxes Steirer, K.; Young, J. L.; Koldemir, U.; Sellinger, A.; Turner, J. A.; Deutsch, T. G.; Olson, D. C., Phosphonic Acid Modification of $GaInP_2$ Photocathodes Toward Unbiased Photoelectrochemical Water Splitting, ACS Appl. Mater. Interfaces 2015, 7(21), 11346-11350.

[12] Liang, Z.; Hou, H.; Fang, Z.; Gao, F.; Wang, L.; Chen, D.; Yang, W. Hydrogenated TiO_2 Nanorod Arrays Decorated with Carbon Quantum Dots toward Efficient Photoelectrochemical Water Splitting, ACS Appl. Mater. Interfaces 2019, 11(21), 19167-19175.

[13] Govatsi, K.; Seferlis, A.; Yannopoulos, S. N.; Neophytides, S. G.; The Photo-Electrokinetics of the O_2 Evolution Reaction on ZnO Nanorods, Electrochim. Acta 2019, 298, 587-598.

[14] de Respinis, M.; De Temmerman, G.; Tanyeli, I.; van de Sanden, M. C. M.; Doerner, R. P., Baldwin, M. J.; van de Krol, R., Efficient Plasma Route to Nanostructure Materials: Case Study on the Use of m-WO3 for Solar Water Splitting, ACS Appl. Mater. Interfaces 2013, 515, 7621-7625.

[15] Wiktor, J.; Pasquarello, A., Electron and Hole Polarons at the $BiVO_4$–Water Interface, ACS Appl. Mater. Interfaces 2019, 11 (20), 18423-18426.

[16] Shi, Y.; Gimbert-Suriñach, C.; Han, T.; Berardi, S.; Lanza, M.; Llobet, A., CuO-Functionalized Silicon Photoanodes for Photoelectrochemical Water Splitting Devices, ACS Appl. Mater. Interfaces 2016, 81, 696-702.

[17] Kim, J. S.; Cho, S. W.; Deshpande, N. G.; Kim, Y. B.; Yun, Y. D.; Jung, S. H.; Kim, D. S.; Cho, H. K., Toward Robust Photoelectrochemical Operation of Cuprous Oxide Nanowire Photocathodes Using a Strategically Designed Solution-Processed Titanium Oxide Passivation Coating, ACS Appl. Mater. Interfaces 2019, 11 (16) 14840-14847.

[18] Rongé, J.; Deng, S.; Pulinthanathu Sree, S.; Bosserez, T.; Verbruggen, S. W.; Kumar Singh, N.; Dendooven, J.; Roeffaers, M.B.J.; Taulelle, F.; De Volder, M.; Detavernier, C.; Martens, J. A. Air-based Photoelectrochemical Cell Capturing Water Molecules from Ambient Air for Hydrogen Production, RSC Adv. 2014, 4 (55), 29286-29290.

[19] Modestino, M.A.; Dumortier, M.; Hosseini Hashemi, S.M.; Haussener, S.; Moser, C.; Psaltis, D. Vapor-Fed Microfluidic Hydrogen Generator, Lab Chip 2015, 15 (10), 2287-2296.

[20] Amano, F.; Mukohara, H.; Shintani, A.; Tsurui, K. Solid Polymer Electrolyte-Coated Macroporous Titania Nanotube Photoelectrode for Gas-Phase Water Splitting. ChemSusChem 2018, 12 (9), 1925-1930.

[21] Kumari, S.; Turner White R.; Kumar, B.; Spurgeon, J. M.; Solar Hydrogen Production from Seawater Vapor Electrolysis, Energ Environ Sci. 2016, 9 (5), 1725-1733.

[22] Stoll, T.; Zafeiropoulos, Z.; Tsampas, M. N. Solar Fuel Production in a Novel Polymeric Electrolyte Membrane Photoelectrochemical (PEM-PEC) Cell with a Web of Titania Nanotube Arrays as Photoanode and Gaseous Reactants, Int. J. Hydrog. Energy 2016, 41 (40), 17807-17817.

[23] Stoll, T.; Zafeiropoulos, G.; Dogan, I.; Genuit, H.; Lavrijsen, R.; Koopmans, B.; Tsampas, M. N. Visible-Light-Promoted Gas-Phase Water Splitting using Porous $WO_3/BiVO_4$ Photoanodes, Electrochem. Commun. 2017, 82, 47-51.

[24] Zafeiropoulos, G.; Stoll, T.; Dogan, I.; Mamlouk, M.; van de Sanden, M. C. M.; Tsampas, M. N., Porous Titania Photoelectrodes Built on a Ti-Web of Microfibers for Polymeric Electrolyte Membrane Photoelectrochemical (PEM-PEC) Cell Applications, Sol Energ Mat and Sol C. 2018, 180, 184-195.

[25] Georgieva, J.; Armyanov, S.; Poulios, I.; Sotiropoulos, S.; An All Solid Photoelectrochemical Cell for the Photooxidation of Organic Vapours under Ultraviolet and Visible Light Illumination, Electrochem Commun. 2009, 11, 1643-1646.

[26] Georgieva, J.; Armyanov, S.; Poulios, I.; Jannakoudakis, A. D.; Sotiropoulos, S. Gas Phase Photoelectrochemistry in a Polymer Electrolyte Cell with a Titanium Dioxide/Carbon/Nafion Photoanode, Electrochem. Solid-State Lett. 2010, 13 (10), P11-P13.

[27] Iwu, K. O.; Galeckas, A.; Kuznetsov, A. Y.; Norby, T. Solid-state Photoelectrochemical H_2 Generation with Gaseous Reactants, Electrochim. Acta 2013, 97, 320-325.

[28] Xu, K.; Chatzitakis, A.; Vøllestad, E.; Ruan, Q.; Tang, J.; Norby, T., Hydrogen from Wet Air and Sunlight in a Tandem Photoelectrochemical Cell, Int. J. Hydrog. Energy 2019, 44 (2), 587-593.

[29] Bosserez, T.; Ronge, J.; van Humbeeck, J.; Haussener, S.; Martens, J. Design of Compact Photoelectrochemical Cells for Water Splitting, Oil Gas Sci Technol. 2015, 70 (5), 877–889.

[30] Amano, F.; Shintani, A.; Tsurui, K.; Hwang, Y. M. Fabrication of Tungsten Trioxide Photoanode with Titanium Microfibers as a Three Dimensional Conductive Back Contact, Mater. Lett. 2017, 199, 68–71.

[31] Aricò, A.; Girolamo, M.; Siracusano, S.; Sebastian, D.; Baglio, V.; Schuster, M. Polymer Electrolyte Membranes for Water Photo-Electrolysis, Membranes, 2017, 7 (2), 2 (1-16).

[32] Carmo, M.; Fritz, D.L.; Mergel, J.; Stolten, D. A Comprehensive Review on PEM Water Electrolysis, Int. J. Hydrog. Energy 2013, 38 (12), 4901-4934.

[33] Kusoglu, A.; Weber, A.Z. New Insights into Perfluorinated Sulfonic-Acid Ionomers, Chem. Rev. 2017, 117 (3), 987-1104.

[34] Siracusano, S.; Baglio, V.; Stassi, A.; Merlo, L.; Moukheiber, E.; Arico', A. S. Performance Analysis of Short-Side-Chain Aquivion® Perfluorosulfonic Acid Polymer for Proton Exchange Membrane Water Electrolysis, J Membrane Sci. 2014, 466, 1-7.

[35] Dionigi, F.; Vesborg, P. C. K.; Pedersen, T.; Hansen, O.; Dahl, S.; Xiong, A.; Maeda, K.; Domen, K.; Chorkendorff, I. Gas Phase Photocatalytic Water Splitting with $Rh_{2-y}Cr_yO_3$/GaN:ZnO in μ-reactors, Energ Environ Sci. 2011, 4 (8), 2937-2942.

[36] O'Hayre, R.; Prinz, F.B. The Air/Platinum/Nafion Triple-Phase Boundary: Characteristics, Scaling, and Implications for Fuel Cells, J. Electrochem. Soc. 2004, 151 (5), A756-A762.

[37] Barbir, F. PEM Fuel Cells: Theory and Practice, 2nd Edition, Academic press, 2013

[38] Tsampas, M. N.; Brosda, S.; Vayenas, C. G. Electrochemical impedance spectroscopy of fully hydrated Nafion membranes at high and low hydrogen partial pressures, Electrochim. Acta 2011, 56, 10582-10592.

[39] Barsoukov, E.; Macdonald, J.R. Eds., Impedance Spectroscopy: Theory, Experiment, and Applications, Wiley-Interscience, 2005.

[40] Yadav, R.; Fedkiw, P.S. Analysis of EIS Technique and Nafion 117 Conductivity as a Function of Temperature and Relative Humidity, J. Electrochem. Soc. (2012) 159 (3) B340-B346

[41] Li, N.; Song L.; Bießmann, L.; Xia, S.; Ohm, W.; Brett, C.J.; Hadjixenophontos, E.; Schmitz, G.; Roth, S.V.; Müller-Buschbaum, P. Morphology Phase Diagram of Slot-Die Printed TiO2 Films Based on Sol–Gel Synthesis, Adv. Mater. Interfaces 2019, 1900558, 1-9

[42] Cheng, Y.J.; Gutmann J.S. Morphology Phase Diagram of Ultrathin Anatase TiO2 Films Templated by a Single PS-b-PEO Block Copolymer, J. Am. Chem. Soc. 2006, 128, 4658-4674

[43] Amano, F.; Shintani, A.; Mukohara, H.; Hwang, Y.M.; Tsurui, K. Photoelectrochemical Gas–Electrolyte–Solid Phase Boundary for Hydrogen Production From Water Vapor, Front Chem. 2018, 6 (598).

[44] Amano, F.; Mukohara, H.; Sato, H.; Ohno, T. Photoelectrochemical Water Vapor Splitting using an Ionomer-Coated Rutile TiO_2 Thin Layer on Titanium Microfiber Felt as an Oxygen-Evolving Photoanode, Sustain Energ Fuels 2019, 3, 2048-2055.

[45] Rattanachai, Y.; Rintramee, K.; Rattanasuporn, S.; Supruangnet, R. Characterization of Nafion XL Membrane for PEMFC after VUV Degradation and Titanium Nitride Coating, Nucl Instrum Meth B 2018, 436, 292-297.

[46] Melo, L. G. A.; Hitchcock, A. P.; Susac, D.; Stumper, J.; Berejnov, V. Effect of UV radiation Damage in Air on Polymer Film Thickness, Studied by Soft X-ray Spectromicroscopy, Phys. Chem. Chem. Phys. 2018, 20 (24), 16625-16640.